Numerical Investigation of Acoustic Refraction

Joseph D. Baum*
Naval Research Laboratory, Washington, DC
and
Jay N. Levine†
Edwards Air Force Base, California

The objective of our research project was to understand the physical mechanisms by which energy is exchanged between the mean and acoustic flowfields in resonant combustion chambers (in particular, solid rocket motors); specifically, vortex shedding and the so-called "flow turning" effect. This paper details efforts, to date, to develop the computational capability to properly address such problems and reports progress made toward the understanding of acoustic refraction. Acoustic-mean flow interactions are investigated via a solution of the time-dependent, compressible Navier-Stokes equations. A comparison of explicit and implicit schemes demonstrate the superiority of the implicit scheme for the present application. An extensive study is conducted to determine the current state of the art in the modeling of nonreflective boundary conditions for low Mach number sheared flows. Results obtained demonstrate that all models result in reflection of incident waves. Thus, it is decided to discontinue the solution when the wavefront starts reflecting from the downstream boundary. Acoustic refraction study results demonstrate the ability of the developed methodology to calculate refraction phenomenon and its dependence on the direction of propagation, frequency, and Mach number. The interaction between the mean and the acoustic flowfields inside the acoustic boundary layer is shown to result in the excitation of mean flow velocity at the edge of the acoustic boundary layer, a phenomenon better known as Richardson's annular effect. Additional results demonstrate the spatial and radial growth of pressure and axial velocity mean shifts, indicating mean flow excitation by the acoustic flow. Finally, complex flow processes are shown to occur as the acoustic field at a given axial location undergoes a sign change.

Introduction

THIS paper is directed toward the understanding and modeling of vortex shedding and flow turning, two of the operative physical mechanisms responsible for energy exchange between the mean and acoustic flowfields in solid rocket combustion chambers.

Pressure oscillations have caused significant operational problems in several solid propellant rocket motors. Such oscillations represent a condition of combustion instability. In some cases, small amplitude oscillations indigenous to the motor chamber (i.e., random noise produced by combustion or turbulence) can be amplified by interaction with the burning solid propellant or by energy transfer from the mean gas flow in the chamber. These oscillations can alter the thrust time characteristics of the motor, affect the operation of sensitive electronic equipment, and, in extreme cases, produce significant mean pressure shifts that result in motor case failure.

The growth or decay of random small-amplitude pressure oscillations is determined by a delicate balance between the driving and damping of oscillatory energy in the motor chamber. The processes that dissipate acoustic energy include convection and radiation of acoustic energy through the nozzle (nozzle damping), the viscous and thermal losses produced by interaction of the condensed phase combustion products with the combustion gases (particle damping), the nonlinear viscoelastic characteristics of the grain case (structural damping), viscous losses in the gas phase and at inert surfaces, gas-phase vibrational relaxation effects, radiation of energy through the motor case, and inelastic acceleration of combustion products leaving the propellant surface (flow turning). The primary source of oscillatory energy considered to date has been the response of the propellant combustion zone to acoustic pressure and acoustic velocity oscillations (termed pressure and velocity coupling, respectively). Other sources of energy include the combustion of incompletely reacted products in the chamber, distributed combustion of metal droplets in the gas phase, and conversion of mean flow energy to acoustic energy due to vortex shedding. The determination (both by theoretical predictions and experimental measurements) of the various energy sources and sinks in a combustion chamber is critical to our ability to predict, a priori, the stability characteristics of proposed solid rocket designs.

The objective of our research project was to seek an understanding of the physical mechanisms by which energy is exchanged between the mean and acoustic flowfields in resonant combustion chambers; specifically, vortex shedding and the so-called flow-turning effect. The present paper will detail efforts, to date, to develop the computational ability to address such problems and will report progress made toward the understanding of acoustic refraction. Energy exchange through flow turning and vortex shedding will be the subject of future studies.

Flow Turning

The term flow turning describes the loss of acoustic energy accompanying the flow of combustion products inward through the lateral boundary of a combustion chamber containing longitudinal acoustic waves. The mean flow of solid propellant combustion products entering normal to the surface must turn to the axial direction parallel to the boundary; simultaneously, each fluid element of the mean flow must acquire acoustic energy. It is this second process, involving the irreversible action of the unsteady field in the chamber on the

Presented, in part, as Paper 86-0533 at the AIAA 24th Aerospace Sciences Meeting, Reno, NV, Jan. 6–9, 1986; received July 25, 1986; revision received April 24, 1987.

*Laboratory for Computational Physics and Fluid Dynamics.
†Air Force Rocket Propulsion Laboratory/DYCC.

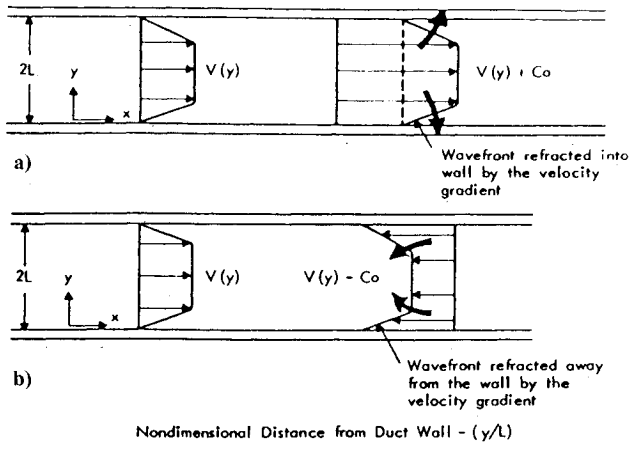

Fig. 1 (a) Schematic of downstream sound propagation and (b) schematic of upstream sound propagation.

entering flow, that has been hypothesized to be a loss of energy for the existing acoustic field. This energy loss is often referred to as flow-turning loss because turning of the mean flow is necessarily involved. However, it is really a rate of energy loss, proportional to the velocity of the incoming flow perpendicular to the boundary.

The modeling of flow turning involves multidimensional, rotational, and viscous flow effects on widely varying distance scales. These effects only increase the difficulty of modeling this problem due to difficulties in both analytical and numerical procedures. Lack of a basic fundamental theory of mean flow-acoustic interactions has resulted in disagreement among researchers[1,2] about a very basic point; namely, is flow turning a surface effect, volume effect, or both? The experimental measurement of this acoustic energy loss mechanism is difficult since this effect usually appears in conjunction with other gain and loss mechanisms and cannot be isolated. An experimental investigation of the flow-turning losses associated with the injection of steady lateral flow of cold air into a rectangular duct containing longitudinal acoustic waves was conducted by Hersh.[3] This experiment was designed to simulate injection of hot combustion products into a combustion chamber. The results indicated that the flow-turning process absorbs sound (i.e., damping of acoustic energy). A one-dimensional model developed by Hersh seriously underpredicted the measured acoustic energy losses. Hersh speculated[4] that in addition to the flow-turning absorption, there is another energy absorption mechanism related to acoustic refraction. Due to refraction by the mean flow velocity gradients, the sound pressure near the side wall increases, thereby enhancing the acoustic energy absorption by the finite admittance walls.

Acoustic Refraction

When sound waves propagate in a moving medium (i.e., with a coexisting mean flow), the main physical processes affecting their propagation, in the absence of viscosity and thermal conduction, are convection and refraction. The sound is convected by the moving medium at its local velocity. In the presence of a sheared mean flow, local convection velocities are a function of position. This results in excitation of pressure gradients in the radial direction, which, in turn, results in the excitation of radial velocities. Thus, for the case of flow in a rigid tube, when the sound wave travels with the mean flow (downstream), the effect of velocity gradients is to refract the sound toward the wall. When the sound propagates against the mean flow (upstream), the effect of radial velocity gradient is to refract the sound toward the centerline. Schematics of downstream and upstream sound propagation are shown in Figs. 1a and 1b, respectively.

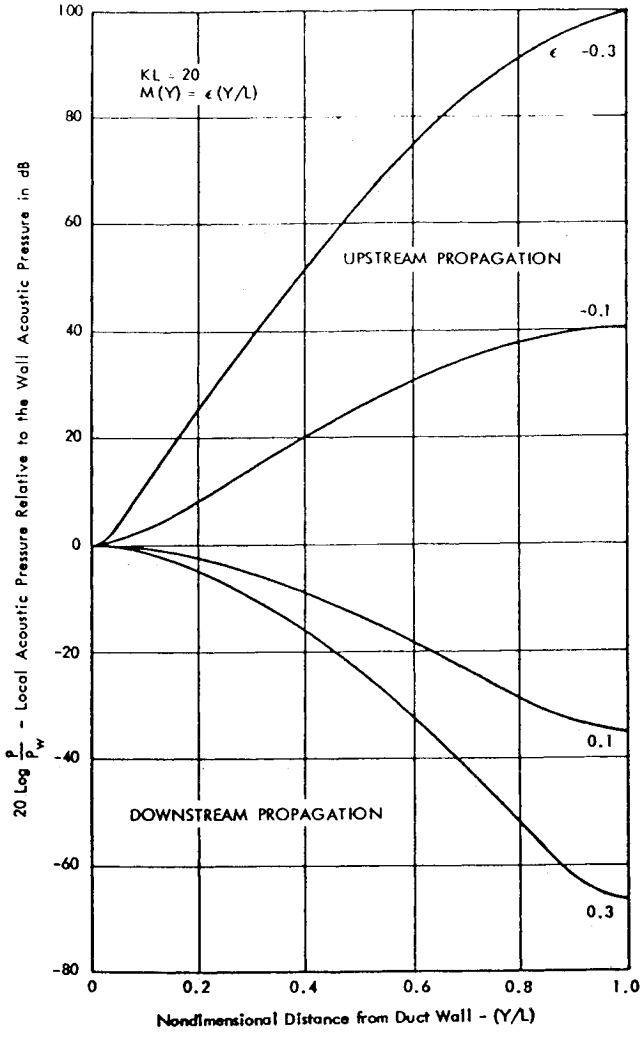

Fig. 2 Effect of flow gradient on the plane-wave acoustic pressure distribution across a rectangular duct for $KL = 20$.

Previous research efforts to model and understand acoustic refraction phenomenon utilized linearized models.[5-8] It is possible that very important second-order nonlinear effects are excluded. For fully developed duct flow, the combined linearized continuity and momentum equations yield.

$$\frac{1}{c_0^2}\frac{\partial^2 p}{\partial t^2} = (1-M^2)\frac{\partial^2 p}{\partial x^2} + \frac{\partial^2 p}{\partial y^2} - \frac{2M}{c_0}\frac{\partial^2 p}{\partial x\,\partial t} + 2\rho_0 c_0 \frac{dM}{dy}\frac{\partial V}{\partial x} \tag{1}$$

where u, v, p, and ρ are the acoustic excitations of axial velocity, normal velocity, pressure, and density. V is the mean velocity in the duct, and $M = V/c_0$. The last term on the right-hand side yields the effect of refraction.

The first linear analysis to consider the effect of shear flow on the propagation and attenuation of sound in a hard wall duct was restricted to downstream propagation only.[5] The study showed that the pressure distribution of an initially plane wave was significantly distorted. The acoustic pressure at the wall was calculated to be 90 dB larger than the pressure at the centerline. The study also indicated that acoustic refraction increases with mean flow Mach number and with the frequency of the oscillations. In succeeding studies,[6-8] the linearized treatment was extended to treat sound propagation upstream in an infinitely long rigid duct as well as the effect of

varying shear layer thickness. Some of the results obtained[6] are shown in Fig. 2 for the case of a constant velocity gradient across the duct. E is the centerline Mach number, K is the wave number in the axial direction, L is the duct half-width, and Y is the distance from the duct wall. It is shown that for upstream sound propagation in a duct with a centerline Mach number of 0.1, the centerline acoustic pressure was 40 dB larger than the acoustic pressure at the wall. When the wave propagated downstream, the pressure level at the wall was 36 dB larger than the pressure at the centerline. The study also showed that all the various perturbation techniques yield virtually the same results. Linear analysis results[5,6] indicated that for a mean flow with a one-seventh power law distribution and centerline Mach numbers in the range of 0.05 through 0.10 (typical centerline Mach numbers in solid motor chambers), the acoustic pressure amplitude near the propellant surface may be twice as high as the acoustic pressure amplitude at centerline. Although nonlinear effects can be expected to reduce significantly the actual refractive enhancement of the near wall pressure, these results indicate that acoustic refraction, which has been virtually ignored in solid rocket stability analyses, may actually have quite important effects. This results from the fact that both the steady and transient response of the burning solid propellant are dependent on the amplitude of the pressure and velocity oscillations near the burning surface.

An experiment to measure acoustic refraction effects is currently in progress.[9] In this experiment, air is blown through a long rigid tube in which a plane wave is excited at the inlet. The mass flux through the tube is varied, resulting in a centerline Mach number variation from 0.038 to 0.10. The results, to date, indicate that the acoustic pressure is amplified near the pipe wall; the degree of amplification increases with Mach number. With a centerline Mach number of 0.1 ($R_e = 2.7 \times 10^5$), the measurements indicate a near wall acoustic pressure amplification of 40%. Such an increase in acoustic pressure amplitude may be critical for motor stability analysis. The discrepancy between the linear theory and the experimental data may possibly result from nonlinear mean flow-acoustic field interactions, which will tend to damp acoustic pressure growth near the walls; processes that are not modeled by the linear analysis.

Numerical Solution

Under the current research program, two two-dimensional axisymmetric Navier-Stokes solvers were acquired and modified for the investigation of acoustic refraction. The first was the MINT implicit code. The code solves the compressible Reynolds-averaged Navier-Stokes equations using an efficient, noniterative, time-dependent linearized block implicit (LBI) scheme.[10-12] The governing equations are written in cylindrical polar coordinates as follows:

$$\frac{\partial \vec{U}}{\partial t} + \frac{\partial \vec{E}}{\partial x} + \frac{1}{r}\frac{\partial (r\vec{F})}{\partial r} = \vec{H} \tag{2}$$

where

$$\vec{U} = \begin{pmatrix} \rho \\ \rho u \\ \rho v \\ \rho e \end{pmatrix}, \quad \vec{E} = \begin{pmatrix} \rho u \\ \rho u^2 - \sigma_{xx} \\ \rho uv - \tau_{rx} \\ \rho ue - u\sigma_{xx} - v\tau_{xr} - \kappa T_r \end{pmatrix}$$

$$\vec{F} = \begin{pmatrix} \rho v \\ \rho uv - \tau_{rx} \\ \rho v^2 - \sigma_{rr} \\ \rho ve - v\sigma_{rr} - u\tau_{xr} - \kappa T_r \end{pmatrix}, \quad \vec{H} = \begin{pmatrix} 0 \\ 0 \\ \dfrac{-\tau_{\theta\theta}}{r} \\ 0 \end{pmatrix}$$

$$\sigma_{xx} = (2\mu + \lambda)\frac{\partial u}{\partial x} + \lambda\left(\frac{v}{r} + \frac{\partial v}{\partial r}\right) - p$$

$$\sigma_{rr} = (2\mu + \lambda)\frac{\partial v}{\partial r} + \lambda\left(\frac{v}{r} + \frac{\partial u}{\partial x}\right) - p$$

$$\tau_{\theta\theta} = (2\mu + \lambda)\frac{v}{r} + \lambda\left(\frac{v}{r} + \frac{\partial u}{\partial x}\right) - p$$

and

$$\tau_{xr} = \tau_{rx} = \mu\left(\frac{\partial u}{\partial r} + \frac{\partial v}{\partial x}\right)$$

The dependent variables for this system of equations are $U(\rho, \rho u, \rho v, \rho e)$. Sutherland's viscosity equation and the equation of state and Prandtl number (Pr) are specified to close this system of equations. The current model utilizes either a turbulent kinetic energy-algebraic length scale ($k - l$) model[13] or a transport turbulence ($k - \epsilon$) model.[14] The latter includes modifications[15] that allow the $k - \epsilon$ model to be utilized throughout the entire viscous sublayer without any wall function assumptions. The resulting code was verified by comparing the predictions to experimental data[16] for flat plate boundary-layer flows with and without wall transpiration. For a complete description of the equations solved and the turbulence models used, see Ref. 15.

The first explicit code was developed by Shang[17-19] for solving time-dependent, compressible Navier-Stokes equa-

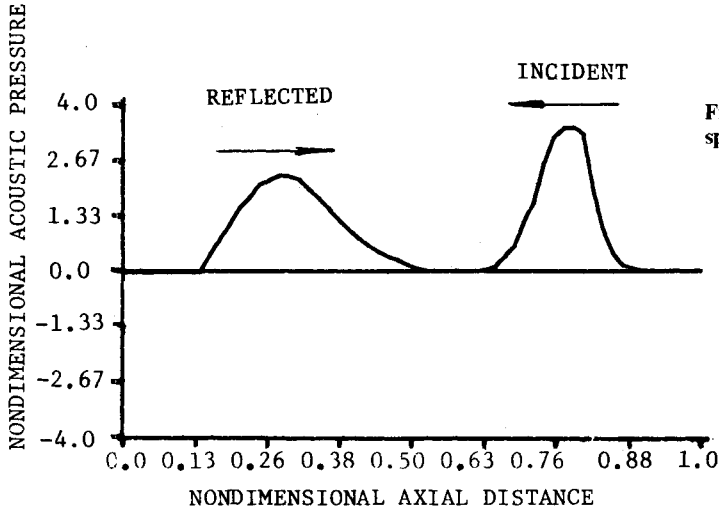

Fig. 3 Study of nonreflecting boundary conditions; upstream boundary: specify t, u, v, extrapolate p.

tions. The $k-\epsilon$ model is utilized in this algorithm. The code utilizes the MacCormack explicit and unsplit scheme[20] as the numerical solution procedure. The algorithm allows variation of the Courant-Friedrichs-Lewy (CFL) number in the range of 0.15 to 0.85. The calculations were performed using a CFL number of 0.5 (in which case the calculation of CFL number is based on the smallest size grid). For the present investigation, a no-slip boundary condition is applied to the outer duct wall and a symmetric boundary condition applied to the duct centerline.

Another explicit code considered was VNAP-2.[21,22] The code employs the unsplit MacCormack scheme to compute the flow at the interior grid points. The governing equations are solved in nonconservative form. Boundary surfaces are calculated using a second-order accurate reference-plane characteristic scheme, combined with a nonreflective formulation of the boundary conditions to be described later.

Boundary Condition Treatment

The linear analysis study just described demonstrated the importance of having a single family of traveling acoustic waves in the system, traveling either upstream or downstream. While waves traveling downstream will channel acoustic energy toward the wall, waves traveling upstream will channel energy toward the centerline. Thus, it is obvious that the study of acoustic energy redistribution due to refraction is enormously simplified when only one family of waves exists in the system at any time. This conclusion holds for both the experimental and computational investigations. In Hersh's experiment, a special muffler was installed at a large distance downstream of the test section to prevent reflection from the end of the tube. In the computational investigation, an effort was made to develop nonreflective boundary conditions to avoid this problem.

The system of governing equations for subsonic flow is classified as an incomplete parabolic type, a mixed initial value-boundary value problem.[23] For two-dimensional subsonic flows, this problem requires four inflow boundary conditions and three outflow boundary conditions. However, in the limit when the characteristic Reynolds number approaches infinity, the governing equations degenerate into the Euler equations, in which case the system becomes the quasi-linear hyperbolic type and the necessary boundary conditions consist of three on the inflow boundary and one at the outflow boundary.[24]

The fundamental problem in treating subsonic outflow boundary conditions is that information about the flow outside the computational domain (i.e., downstream of the exit plane) is required in order to properly calculate the flow at the exit plane. In an attempt to avoid the creation of nonphysical boundary conditions, several approximations have been developed. An assumption frequently used is that at a distance sufficiently far downstream, the flow is essentially inviscid, and thus it is possible to use the far-field condition of a hyperbolic system of equations.[25,26] Another assumption often used is an approximation of the outgoing characteristic variable by extrapolation.[27] This type of low-order extrapolation seems to produce instabilities in the flow. A method to resolve this problem was suggested by Boris et al.[28] The solution utilizes guard cells outside the computational domain; cells that transmit information to the exit plane on the conditions downstream of the exit. This formula incorporates a zero-order approximation and a slow local relaxation toward the known ambient value at a distance far downstream.

Several types of nonreflecting boundary conditions were tested with the explicit and the implicit codes. The test case consisted of perturbing a fully developed turbulent pipe flow (one-seventh power law describing the mean flow, $R_e = 1.1 \times 10^5$) with a plane acoustic wave originating at either side of the tube. Due to the strongly viscous nature of the flow, all the models that are based on assuming essentially inviscid flow failed. The results of this study indicated the complexities of the proper imposition of boundary conditions that do not result in the generation of physically erroneous results.

As just indicated, three boundary conditions have to be specified at the upstream boundary. To test the reflective quality of the proposed boundary conditions, upstream traveling pulses were generated at the downstream boundary. When the density (ρ) and the axial and radial components of the velocity (u and v, respectively) were specified, and the zero-order approximation is used for the pressure, the wave reflected in a "like" manner, i.e., the compression wave was reflected as a compression wave of identical magnitude, and the expansion wave was reflected as an expansion wave, simulating a "hard wall" type of reflection, as shown in Fig. 3. Examination of the boundary conditions imposed indicates that by specifying a constant axial inlet velocity, the perturbed (i.e., acoustic) velocity component u' equals zero. By imposing $\partial p/\partial x = 0$ on the upstream boundary condition (where x is the axial direction), the implied boundary condition on the perturbed component of the pressure is $\partial p'/\partial x = 0$. These two conditions combined (i.e., $u' = 0$, $\partial p'/\partial x = 0$) describe an acoustic boundary condition for a hard wall in complete agreement with the computational results. When the pressure (p), radial velocity (v), and temperature (T) are imposed on the upstream boundary, the reflection is of an unlike manner (i.e., a compressive traveling wave is reflected as a traveling expansion wave and vice versa), as shown in Fig. 4. Analysis of this boundary condition indicates that by holding the pressure constant, the acoustic boundary condition is set to $p' = 0$. If we use a zero-order extrapolation for the axial velocity, the imposed acoustic boundary condition is $\partial u'/\partial x$

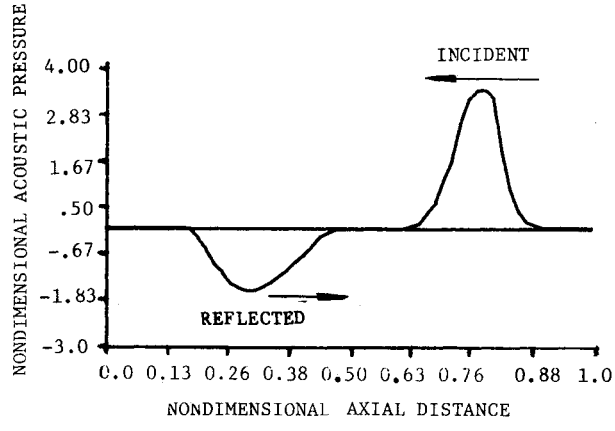

Fig. 4 Study of nonreflecting boundary conditions; upstream boundary; specify p, t, v, extrapolate u.

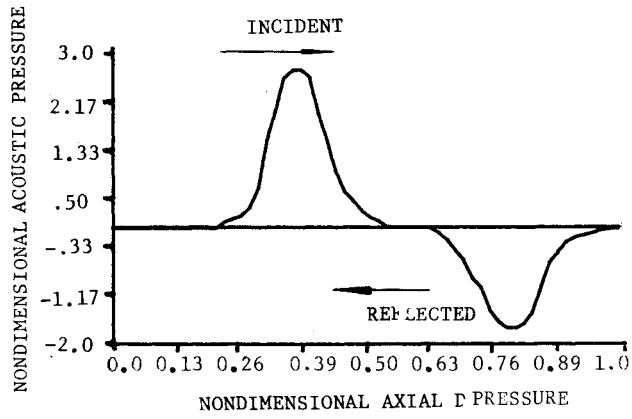

Fig. 5 Study of nonreflecting boundary conditions; downstream boundary: specify p, extrapolate t, u, v.

= 0. This combination describes acoustic reflection from an open end of a tube (i.e., a pressure node at the exit), for which the known solution is identical to the results obtained with the numerical code.

A third type of boundary condition at the head end specifies the total pressure (P_T), total temperature (T_T), and the angle of the inlet flow. This boundary condition results in a reflection that is almost identical to the reflection obtained by specifying p, v, and T (Fig. 4). Since these tests were conducted at low Mach numbers, p is virtually identical to P_T. In addition, although P_T is held constant and not p, the variation observed in the inlet Mach number was insignificant, resulting in an almost constant static pressure. Since this type of boundary condition reduces effectively to the previously discussed boundary conditions (i.e., specifying p, v, and T), the similarity of the results should be of no surprise.

Two different types of nonreflective boundary conditions were shown[21] to yield virtually no reflections. They include specifying v and imposing the nonreflecting boundary condition[25] on the axial velocity, and specifying v and imposing the nonreflecting boundary condition on p. These results, however, were obtained for plane waves simulating a one-dimensional flow problem. When applied to a sheared two-dimensional mean flow, reflections were significantly diminished in amplitude but not eliminated. Another interesting scheme[22] combines the nonreflecting boundary condition with the reference plane characteristic scheme (both for the inflow and outflow planes). It is believed that this scheme may further reduce reflections, but will not eliminate them completely.

The discussion just presented describes numerical results obtained for reflection from the inflow plane. A similar numerical experiment was conducted to investigate reflection from the out-flow plane. A downstream traveling compression wave generated at the upstream boundary was reflected as an expansion wave with approximately half the amplitude, as shown in Fig. 5. This may indicate a splitting of the traveling compression wave into a compression wave exiting the computational domain and an expansion wave reflecting into the domain.

Due to the time limitations, it was decided to discontinue the investigation of nonreflecting boundary conditions for low Mach number sheared flows. The problem of reflecting boundary conditions can be circumvented for the investigation of acoustic refraction. For this investigation, it is possible to generate a steady-state flowfield in the tube and then generate a traveling wave at one end of the tube and integrate the solution until the wavefront starts reflecting from the other end.

Numerical Results

The process of choosing a numerical technique which is most suitable for the solution of a given problem involves the comparison of results obtained using the techniques for the solution of other fluid dynamics problems for which solutions are known; ease of implementation for the current problem of interest; numerical accuracy, computational time, etc. The candidate finite-difference integration schemes were examined (based on these criteria) for a test case of fully developed turbulent pipe flow, with an initial velocity profile described by a one-seventh power law, a centerline inlet Mach number of 0.1, and $R_e = 1.1 \times 10^5$. Uniform mesh distribution was employed in the axial direction, while an exponential stretching scheme was utilized in the radial direction to position a fine mesh near the wall. The implicit solution obtained by the MINT code converged to a steady solution (for a 60×60 mesh) in about 150 time steps, compared to about 100,000 time steps with the explicit codes tested, while employing an even finer mesh distribution near the tube wall. When using identical grids, the code requires less than 10% of the computational time required by the explicit codes to reach steady-state solution. In addition, with the very fine resolution near the wall, the solution obtained at the wall using Shang's scheme was less accurate than the solution obtained with the implicit code. Finally, the time-dependent solutions obtained for these test cases utilizing the MINT were correct. Based on the criteria just discussed, the implicit MINT code was demonstrated, at least for the present application, to be superior to the other codes considered, and thus it was utilized in our research effort.

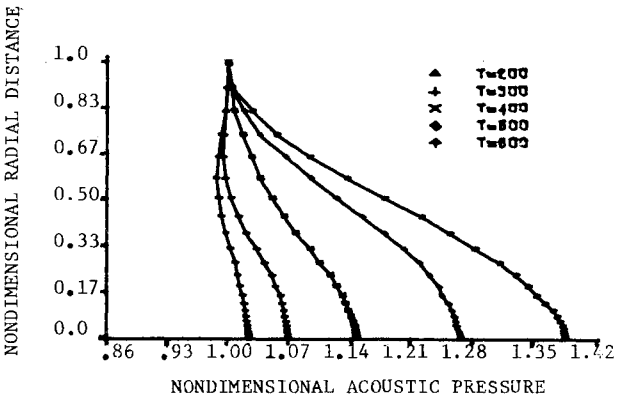

Fig. 6 Time evolution of the radial distribution of acoustic pressure, $f = 6000$ Hz, $M_{c.l.} = 0.1$, downstream propagation.

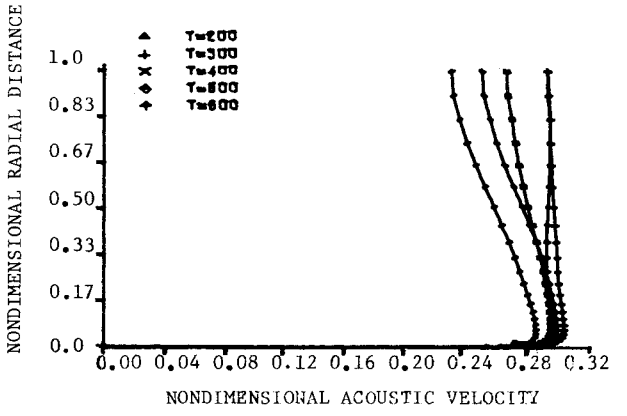

Fig. 7 Time evolution of the radial distribution of acoustic axial velocity, $f = 6000$ Hz, $M_{c.l.} = 0.1$, downstream propagation.

The study of acoustic refraction utilizes a tube with a radius of 0.0508 m (two in.) and a length of approximately three acoustic wavelengths (for any frequency studied). The computational grid consisted of 80 points distributed uniformly in the axial direction and 60 points in the radial direction, with fine mesh resolution near the wall and exponentially stretched mesh toward the centerline. The temperature and the axial and radial components of the velocity are specified at the inlet plane, while constant static pressure was specified at the outflow plane. The pressure at the inlet plane and axial velocity, temperature and radial velocity were extrapolated at the exit plane using a second-order approximation. The calculation is initiated with a one-seventh power law velocity profile at the inlet plane. After convergence to steady state, the pressure and axial velocities at the upstream boundary are perturbed continuously to produce a system of downstream traveling waves in the computational domain. The amplitude of the pressure oscillations was 4% of the mean pressure. Due to the previously demonstrated inadequacy of all currently available nonreflective models for low Mach number sheared flows, the solution was terminated when the front of the initial wave started reflecting from the downstream boundary.

The first test case was conducted at a frequency of 6000 Hz and centerline Mach number equal to 0.1. The time evolution

of the radial distribution of acoustic pressure is shown in Fig. 6. The initial plane wave was distorted rapidly as the wave propagated downstream. After 600 time steps, when the solution was terminated, the amplitude of the acoustic pressure at the wall was 39.5% larger than at centerline. It is interesting to notice that initially ($T = 200$ and $T = 300$), the amplitude of the acoustic pressure at approximately two-third radial distance away from the wall was lower than the amplitude at the centerline. This distortion disappeared at later times when the amplitude of the acoustic pressure increased continuously from the centerline to the wall. The corresponding time evolution of the radial distribution of the axial acoustic velocity is shown in Fig. 7. The initial plane wave was distorted in time. After 600 time steps, the amplitude of axial velocity oscillations near the wall was 31% larger than at centerline. It should be noticed that the amplitude of both pressure and velocity oscillations was reduced in time as the wave propagated downstream, indicating a decrease of acoustic energy contained in the wave. Acoustic energy dissipation may result due to either physical processes or erroneous numerical dissipation (i.e., artificial viscosity effects and accumulative truncation error resulting from the temporal first-order accuracy of the scheme). Investigation of acoustic energy dissipation demonstrated that erroneous numerical dissipation was significantly lower than acoustic energy loss due to physical processes.

Upstream propagation of plane acoustic waves in the presence of a sheared mean flow was investigated by continuously perturbing the pressure and axial velocity at the downstream boundary to produce an upstream traveling wave. After propagating upstream for 600 time steps, the solution (shown in Fig. 8) indicated that the acoustic pressure amplitude at centerline was 54% larger than at the wall. Similarly, the acoustic axial velocity amplitude at the centerline (Fig. 9) was 30% larger than at the wall. For acoustic wave propagation downstream at 3000 Hz, the amplitude of acoustic pressure oscillations near the wall was 6.4% larger than at centerline, while for acoustic wave propagation upstream, the acoustic pressure amplitude at the wall was 8% lower than at centerline (Fig. 10), demonstrating, again, stronger acoustic refraction effects for upstream sound propagation than for downstream propagation. Further reduction of the frequency resulted in even smaller acoustic refraction effects. Finally, refraction dependence on centerline Mach number was investigated by increasing the centerline Mach number from 0.1 to 0.3. With a 3000 Hz frequency of oscillations and for downstream propagation, the acoustic pressure amplitude near the wall was 17% larger than at centerline (Fig. 11), significantly larger than the 6.4% acoustic pressure increase predicted for the 0.1 Mach number test.

The results presented so far were obtained on the Air Force Weapons Laboratory Cray 1-S computer. Many of these calculations were repeated on the more powerful Naval Research Laboratory Cray X-MP/24 computer. The repeat calculations were conducted with approximately twice as many mesh points per wave length; a larger total number of points in the axial direction (currently about 250, for a length of five acoustic wave cycles, for any frequency studied) that, in turn, enabled integration over more wave cycles before the computation was terminated (currently up to six wave cycles); more points in the radial direction (currently approximately 120) and a better distribution of mesh points next to the wall (the first mesh was a distance of 2.5 μm from the wall); and finally, to help overcome the first-order accuracy of the MINT code,

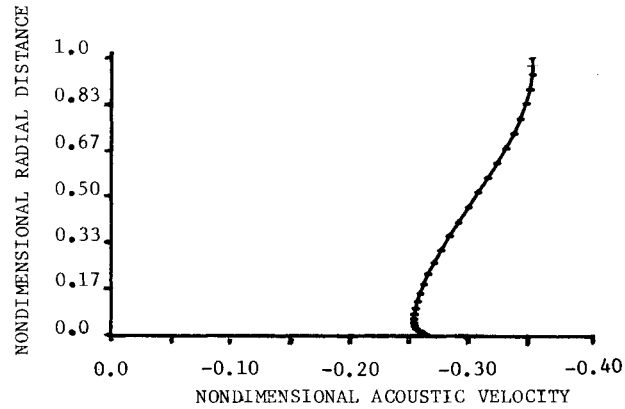

Fig. 9 Radial distribution of axial acoustic velocity, $f = 6000$ Hz, $M_{c.l.} = 0.1$, upstream propagation.

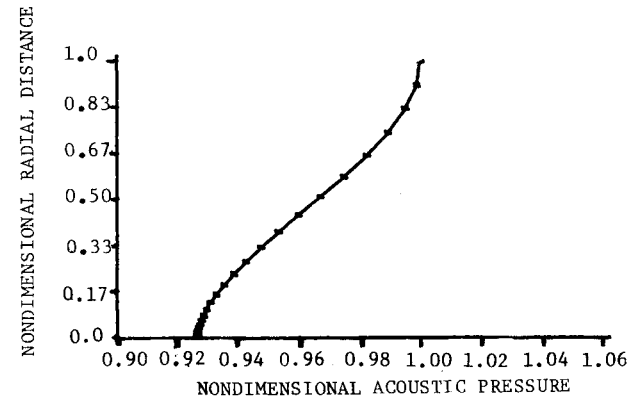

Fig. 10 Radial distribution of acoustic pressure, $f = 3000$ Hz, $M_{c.l.} = 0.1$, upstream propagation.

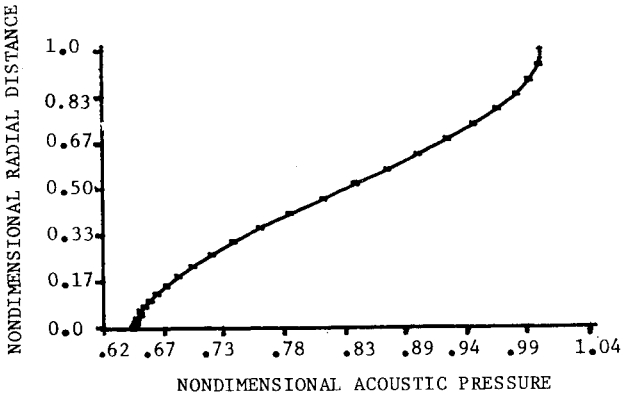

Fig. 8 Radial distribution of acoustic pressure, $f = 6000$ Hz, $M_{c.l.} = 0.1$, upstream propagation.

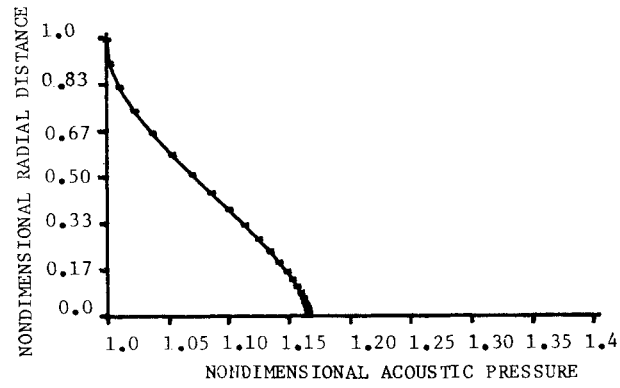

Fig. 11 Radial distribution of acoustic pressure, $f = 3000$ Hz, $M_{c.l.} = 0.3$, downstream propagation.

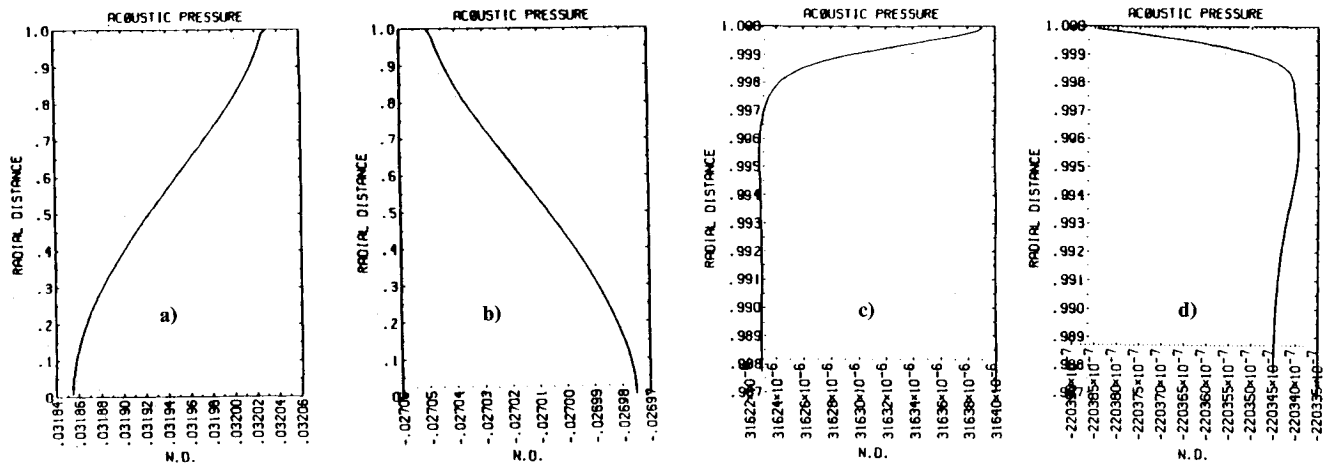

Fig. 12 Radial distribution of acoustic pressure, $f = 1000$ Hz, $Z = 1.32$ m. a) $t = 4.77$ ms; b) $t = 5.32$ ms; c) expanded view, $t = 4.75$ ms; and d) expanded view, $t = 5.24$ ms.

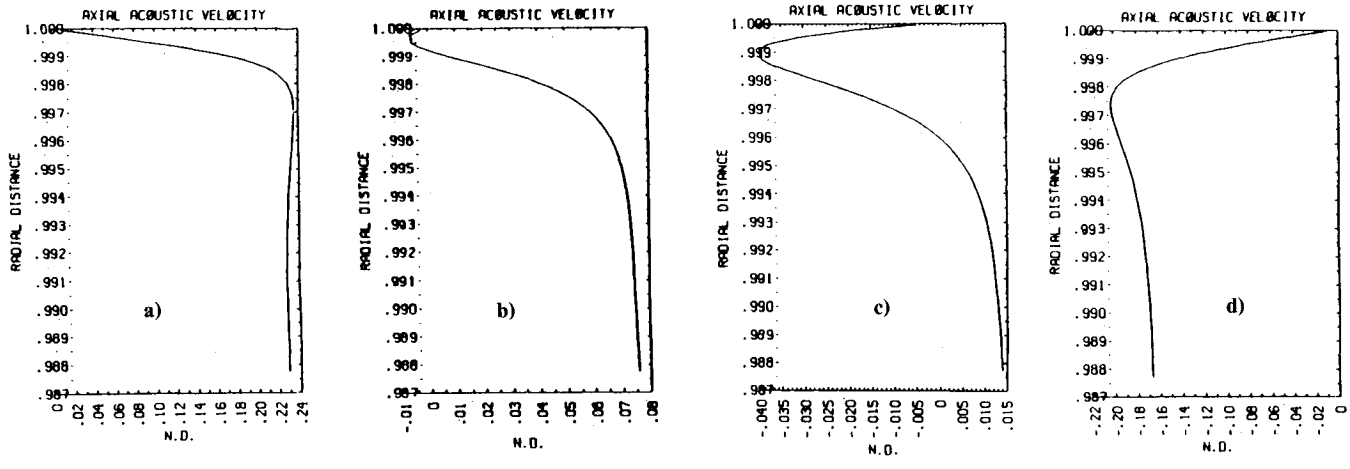

Fig. 13 Radial distribution of axial acoustic velocity, $f = 1000$ Hz, $Z = 1.32$ m. a) $t = 4.75$ ms; b) $t = 4.96$ ms; c) $t = 5.03$ ms; and d) $t = 5.24$ ms.

twice as many time steps per wave cycle are utilized (300 time steps compared to 150 previously). A partially vectorized version of the MINT code was used that was both faster (approximately 3.8 times faster) than the scalar code and, due to improved code architecture, required less storage for the identical grid size. The repeated calculations on the Cray X-MP computer resulted in pressure and axial acoustic velocity values that were not significantly different (within a few percent) from the results obtained on the Cray 1-S computer. This observation does not imply that artificial numerical dissipation (which depends on both spatial and temporal resolution) had been completely eliminated. Nevertheless, it suggests that numerical dissipation constitutes only an insignificant part of the total acoustic energy dissipated as the wave traverses the length of the computational domain.

The new calculations enabled enhanced resolution of the acoustic boundary layer and better simulation of energy exchange processes within the acoustic boundary layer. Several processes have been observed. Due to space and time limitations, only a few of these will be highlighted. Discussion of other results and further analysis of the results emphasized here will be deferred to future publications.

Figures 12 and 13 show radial distributions of acoustic pressure and axial acoustic velocity at an axial station located 1.32 m downstream from the left boundary, for the complete radius of the tube, and for a narrow zone near the wall. This solution was obtained for a traveling wave frequency of 1000 Hz. The radial distance is nondimensionalized by the radius (0.05 m), with the origin at the centerline. Figures 12a and 12b show the radial distribution of acoustic pressure at $t = 4.72$ ms and $t = 5.32$ ms, when the acoustic wave is near its maximum and minimum, respectively, at this location. Notice that acoustic pressure variation across the tube is relatively small, as the maximum acoustic pressure refraction for a downstream propagating wave at 1000 Hz was shown previously to be less than 1%. The increase of acoustic pressure across the acoustic boundary layer (approximately 150 μm at this time) that results from acoustic refraction is demonstrated in the expanded views for both the wave maxima (Fig. 12c) and minima (Fig. 12d).

Figure 13 describes the transition of the axial acoustic velocity from a positive value (downstream directed) to a negative value (upstream directed). At $t = 4.75$ ms (Fig. 13a), the acoustic wave just started decaying from its maximum value. Notice the overshoot of acoustic axial velocity at the edge of the acoustic boundary layer (Richardson's annular effect). At a later time, as the amplitudes of the acoustic pressure and axial velocities are decreasing, a further decrease is observed near the wall (within the acoustic boundary layer). This phenomenon is further enhanced at $t = 4.96$ ms (Fig. 13b), at which time the axial acoustic velocity near the wall becomes negative. At $t = 5.03$ ms (Fig. 13c), the acoustic pressure across the tube is still completely positive, while the axial acoustic velocity is positive everywhere, except near the

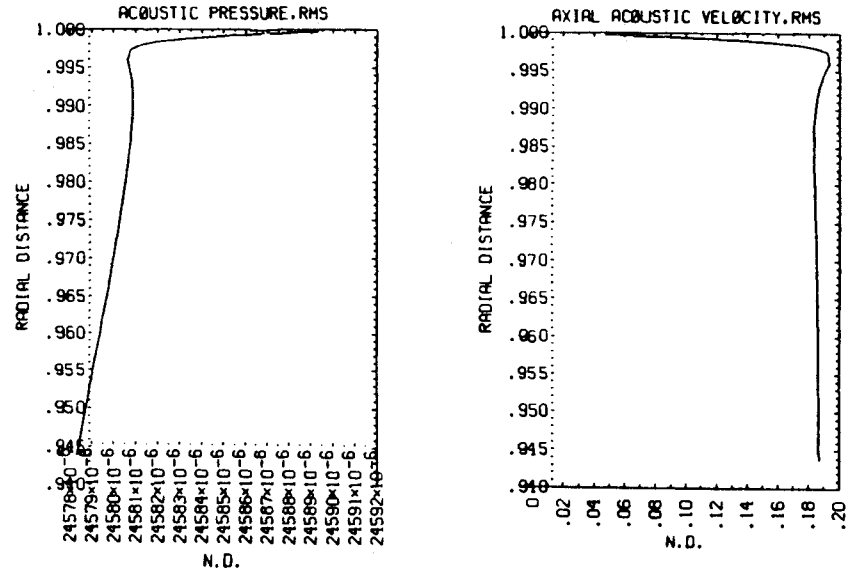

Fig. 14 Radial distribution of root-mean-squared acoustic pressure and axial acoustic velocity, $f = 1000$ Hz, $Z = 0.515$ m.

wall. At this time, the thickness of the newly formed acoustic boundary layer is only 68 μm. Simultaneously, with the formation of a new acoustic boundary layer near the wall (with a negative velocity sign), the previous acoustic boundary layer (with a positive sign and its own overshoot) is propagating further into the core flow, with a thickness of approximately 250 μm (at $t = 5.03$ ms). The acoustic pressure and axial acoustic velocity become negative only at $t = 5.05$ ms. Richardson's annular effect is demonstrated again at $t = 5.24$ ms (Fig. 13d), when the wave is near its minimum.

Another phenomenon observed is the time variation of the acoustic boundary-layer thickness. A new boundary layer is formed near the wall whenever the wave changes its sign. Boundary-layer thickness grows in time to a maximum value of 250 μm, at the next sign change.

To correlate the results obtained with results available in the literature,[29,30] results that are typically in the form of rms values, a computation of the acoustic values obtained at 1000 Hz was performed. A typical result is shown at an axial station located 0.515 m downstream of the left boundary. Figure 14 shows the near wall radial distribution of the acoustic pressure and the axial acoustic velocity. The axial acoustic velocity figure demonstrates Richardson's annular effect. The rms-calculated value for the acoustic boundary-layer thickness is approximately 180 μm, in good agreement with experimental data[29,30] and approximate analysis predictions.[31] The rms-calculated acoustic boundary-layer thickness decreased from 180 μm at 1000 Hz to 120 μm at 6000 Hz, in agreement with experimental trends.[30] In this connection, it should be mentioned that, to the best of our knowledge, these are the first solutions demonstrating either Richardson's annular effect or refraction effects that were obtained via a solution of the complete Navier-Stokes equations.

As noted in the introduction, it was expected that part of the acoustic energy of the waveform would be converted to mean flow energy. Thus, a planar wave introduced at the left boundary should exhibit increasingly larger mean pressure and axial velocity shifts as the wave propagated downstream. Only small mean pressure or axial velocity shifts are observed close to the left boundary, and the axial acoustic velocity and the acoustic pressure are in phase. The situation changes as the wave propagates downstream. The mean pressure at axial station 155 (Fig. 15a) is shifted by approximately 0.25% and the mean axial velocity by 0.2%. The phase shift between these quantities is significant. While these mean shift values seem small, they represent a transfer of 9.1% of the initial acoustic energy to the mean flow energy. In general, the mean pressure shift increases with distance from the inlet and remains constant across the tube cross section at a given axial location. The mean axial velocity shift increases both with distance from the inlet and with distance from the centerline. The radial increase becomes significant only within the acoustic boundary layer. At a distance of 60 μm from the wall, the mean velocity shift increases to 0.32%. Finally, at a distance of 17μm from the wall, the mean velocity is shifted by approximately 0.57% (Fig. 15b), implying that approximately 18% of the initial acoustic energy in this location has been converted to mean flow energy. It is of interest to note that inside the acoustic boundary layer, the phase differences between the axial acoustic velocity and the acoustic pressure increase toward the wall. At the wall, the axial acoustic velocity leads the acoustic pressure by approximately 30–45 deg (in agreement with linear analysis[31]).

Acoustic energy losses can occur due to either viscous dissipation or acoustic energy transfer to mean flow energy. The separation of these losses requires the separation of acoustic properties (those that propagate with the local sound speed) from properties that are convected by the mean flow. The separation of these properties in a flow that involves multidimensional rotational and viscous flow effects has never before been extensively studied or resolved. The most important question, namely the exact definition of acoustic energy in a rotational viscous flow, has been the subject of very recent research investigations.[32] Since the objective of this paper is to present several preliminary results, leaving the calculation of acoustic energy dissipation and conversion to mean flow energy for future reports, it was decided to minimize here any discussion of acoustic energy. Notwithstanding, the simultaneous significant increases of both axial acoustic velocity and acoustic pressure amplitudes near the wall (for downstream propagation) with respect to the corresponding values at centerline (or the opposite trend for upstream propagation) indicate a significant change in the radial distribution of acoustic energy as the wave traverses the tube length. Perturbation-energy calculations (i.e., energy calculation based on perturbed properties) indeed demonstrated redistribution of energy. However, the calculated values combine the acoustic energy redistribution due to acoustic refraction and mean flow energy excitation at the edge of the acoustic boundary layer due to streaming effects. Separation of the perturbed energy into acoustic and excited means flow energies will be performed in the future.

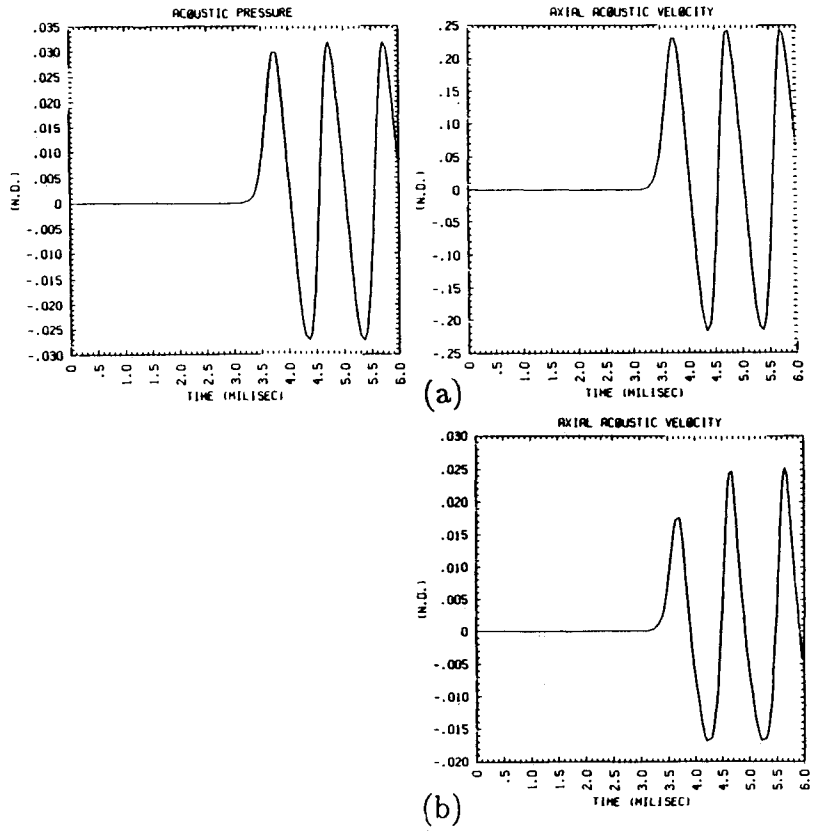

Fig. 15 Time evolution of acoustic pressure and axial acoustic velocity. $f = 1000$ Hz: a) $Z = 1.321$ m. centerline; b) $Z = 1.321$ m. distance to wall = 17μm.

Conclusions

The development of a computational methodology to investigate acoustic energy exchange between the mean and acoustic flowfields through such physical phenomena as acoustic refraction, flow turning and vortex shedding is reported in this paper. Extensive testing of three explicit and implicit Navier-Stokes solvers demonstrated the superiority of the implicit MINT code for the present application. Results obtained with the MINT code demonstrated its ability to handle grid-size ratios of 10000 : 1, converge to a steady-state solution in less than 200 time steps, and obtain time-accurate solutions for time-dependent wave propagation in the tube.

An extensive study was conducted to determine the state of the art in modeling of nonreflective boundary conditions for subsonic sheared flows. The investigation demonstrated that all models result in significant reflections for two-dimensional subsonic waves. Thus, it was decided to study the time evolution of acoustic refraction as the traveling wave traverses the length of the chamber and terminate the solution once the wavefront starts reflecting from the downstream boundary.

The results obtained in the acoustic refraction study indicate that acoustic refraction effects 1) increase with frequency; 2) increase with Mach number; 3) are higher for upstream wave propagation than for downstream wave propagation; and 4) are significantly lower than predicted by the linear theory. The excitation of mean flow at the edge of the acoustic boundary layer, a phenomenon better known as Richardson's annular effect, has been demonstrated. The magnitude of the overshoot at the edge of the acoustic boundary layer and the boundary-layer thickness changed in time during the wave cycle and changed with frequency. In addition, the results obtained demonstrated acoustic streaming effects, specifically mean pressure and axial velocity shifts. The mean pressure shift increased with downstream propagation along the tube and was approximately constant at any axial cross section. The mean axial velocity shift increased with distance from the left boundary and increased significantly within the acoustic boundary layer.

Complex flow phenomena were observed to occur as the acoustic field at a given location transitions from positive acoustic pressure and axial acoustic velocity to negative values, or from a radial acoustic velocity directed toward the wall (positive) to a radial velocity directed toward the centerline (negative velocity). It was shown that the radial acoustic velocity leads the acoustic pressure and axial acoustic velocity by 90 deg and that near the wall the axial acoustic velocity leads the acoustic pressure by approximately 30 deg.

Perturbation-energy calculations demonstrated redistribution of energy. The calculated values combine the acoustic energy redistribution due to acoustic refraction and mean flow energy excitation at the edge of the acoustic boundary layer due to streaming effects. Separation of the perturbed energy into acoustic and excited mean flow energies will be performed in the future.

Based on the results obtained in this study and the experimental results obtained by Hersh, it appears that refraction effects that have not been previously considered in solid motor stability analyses should be incorporated in the models. It appears that this mechanism has a potential to enhance both the acoustic pressure and axial acoustic velocity near the propellant surface, and thus, it may have a significant effect on the propellant transient burn rate.

Acknowledgments

The authors wish to thank J. S. Sabnis of Science Research Associates for his help with the MINT code. Partial funding for this research work was provided by Air Force Office of Scientific Research.

References

[1] Culick, F.E.C., "The Stability of One-Dimensional Motions in a Rocket Motor," *Combustion Science and Technology*, Vol. 7, 1973, pp. 165–175.

[2] Flandro, G.A., "Solid Propellant Admittance Correction," *Journal of Sound and Vibration*, Vol. 36, No. 3, 1974, pp. 297–312.

[3]Hersh, A.S. and Walker, B., "Experimental Investigation of Rocket Motor Flow Turning Losses," AIAA Paper 83–1267, June 1983.

[4]Hersh, A.S. and Walker, B., "Experimental Investigation of Rocket Motor Flow Turning Acoustic Losses," AFRPL TR-84-009, Air Force Rocket Propulsion Lab., Edwards AFB, CA, May 1984.

[5]Pridmore-Brown, D.C., "Sound Propagated in Fluid Flowing in an Attenuating Duct," *Journal of Fluid Mechanics*, Vol. 4, Aug. 1958, pp. 393–406.

[6]Hersh, A.S. and Catton, I., "Effect of Shear Flow on Sound Propagation in Rectangular Ducts," *The Journal of the Acoustical Society of America*, Vol. 50, No. 3, P. 2, Sept. 1971, pp. 992–1003.

[7]Munger, P. and Gladwell, G. M. L., "Acoustic Wave Propagation in a Sheared Flow Contained in a Duct," *Journal of Sound and Vibration*, Vol. 9, No. 1, 1969, pp. 28–48.

[8]Munger, P. and Plumblee, H.E., "Propagation and Attenuation of Sound in an Annular Duct Containing a Sheared Flow," presented at the NASA Basic Noise Research Conference, July 1980.

[9]Hersh, A.S., private communications.

[10]Briley, W.R. and McDonald, H., "Solution of the Multi-Dimensional Compressible Navier-Stokes Equations by a Generalized Implicit Method," *Journal of Computational Physics*, Vol. 24, 1977, pp. 372–397.

[11]Douglas, J. and Gunn, J.E., "A General Formulation of Alternating Direction Methods," *Numerische Mathematics*, Vol. 6, 1964, pp. 428–453.

[12]Briley, W.R. and McDonald H., "On the Structure and Use of Linearized Block Implicit Schemes," *Journal of Computational Physics*, Vol. 34, No. 1, 1980, pp. 54–73.

[13]Launder, B. E. and Spalding, D. B., *Mathematical Models of Turbulence*, Academic Press, New York, 1972.

[14]Launder, B.E. and Spalding, D.B., "The Numerical Computation of Turbulent Flows," *Computer Methods in Applied Mechanics and Engineering*, Vol. 3, 1974, pp. 269–289.

[15]Sabnis, J.S., Gibeling, H.J., and McDonald, H., "Calculation of Motor Internal Flow Field Using an Implicit Navier-Stokes Procedure," AIAA Paper 85–1626, July 1985.

[16]Simpson, R.L., "Characteristics of Turbulent Boundary Layers at Low Reynolds Numbers With and Without Transpiration," *Journal of Fluid Mechanics*, Vol. 42, P. 4, 1970 p. 769–802.

[17]Shang, J.S. and Hankey, W.L., "Numerical Solution of the Navier-Stokes Equations for a Three-Dimensional Corner," *AIAA Journal*, Vol. 15, Nov. 1977, pp. 1575–1582.

[18]Hankey, W.L. and Shang, J.S., "Analysis of Self- Excited Oscillations in Fluid Flows," AIAA Paper 80–1346, July 1980.

[19]Shang, J.S., "Oscillatory Compressible Flow Around a Cylinder," AIAA Paper 82–0098, Jan. 1982.

[20]MacCormack, R.W., "The Effect of Viscosity in Hypervelocity Impact Cratering," AIAA Paper 69–354, April 1969.

[21]Cline, M.C. and Wilmoth, R.G., "Computation of the Space Shuttle Solid Rocket Booster Nozzle Start-Up Transient Flow," AIAA Paper 84–0462, Jan. 1984.

[22]Cline, M.C., "VNAP2: A Computer Program for Computation of Two-Dimensional, Time Dependent, Compressible, Turbulent Flow," LA-8872, Los Alamos National Lab. Rept., Aug. 1981.

[23]Gustaffsson R. and Sundstrom, R., "Incompletely Parabolic Problems in Fluid Dynamics," *SIAM Journal of Applied Mathematics*, Vol. 35, No. 2, Sept. 1978, pp. 343–357.

[24]Steger, J.L. and Pulliam, T.H., "An Implicit Finite Difference Code for Inviscid and Viscous Cascade Flow," AIAA Paper 80–1427, July 1980.

[25]Rudy, D.H. and Strikwerda J.D., "A Nonreflecting Outflow Boundary Condition for Subsonic Navier-Stokes Calculations," *Journal of Computational Physics*, Vol. 36, June 1980, pp. 55–70.

[26]Bayliss, A. and Turkel, E., "Radiation Boundary Conditions for Wake-Like Equations," *Communications on Pure and Applied Mathematics*, Vol. 23, 1980, pp. 707–726.

[27]Gottlieb, D. and Turkel, E., "Boundary Conditions for Subsonic Compressible Navier-Stokes Calculations," *Computers and Fluids*, Vol. 9, 1981, pp. 327–338.

[28]Boris J.P. et al., "Time Dependent, Compressible Simulations of Shear Flows: Tests of Outgoing Boundary Conditions," NRL Memorandum Rept. 5249, Naval Research Lab., Washington D.C., Dec. 1983.

[29]Richardson, P.D., *Dynamics of Real Fluids*, Arnold Ltd., London, 1961.

[30]Richardson, E.G., "The Amplitude of Sound Waves in Resonators," *Proceedings of the Physical Society*, Vol. 50, No. 206, 1928.

[31]Barnett, D., "The Effect of Pressure Pulsations and Vibrations on Fully Developed Pipe Flow," AEDC-TR-80-31, Arnold Engineering Development Center, Aug. 1981.

[32]Myers, M.K., "Generalization and Extension of the Law of Acoustic Energy Conservation in a Nonuniform Flow," AIAA 86–0471, Jan. 1986.